Three-dimensional analysis of abnormal ultrastructural alteration in mitochondria of hippocampus of APP/PSEN1 transgenic mouse

Ki Ju Choi[1,2,†], Mi Jeong Kim[1,†], A Reum Je[1], Sangmi Jun[1], Chulhyun Lee[3], Eunji Lee[4], Mijung Jo[4], Yang Hoon Huh[1,*] and Hee-Seok Kweon[1,*]

[1]*Division of Electron Microscopic Research, Korea Basic Science Institute, 169-148 Gwahangno, Yuseong-gu, Daejeon 305-806, Korea*

[2]*Division of Respiratory Viruses, Center for Infectious Diseases, Korea National Institute of Health, 187 Osong Sangmyeong 2-ro, Gangoe-myeon, Cheongwon-gun, Chungbuk, 363-951, Korea*

[3]*Division of Magnetic Resonance Research, Korea Basic Science Institute, 804-1 Ochang, Chungbuk 363-883, Korea*

[4]*Graduate School of Analytical Science and Technology, Chungnam National University, 79 Daehangno, Daejeon 305-764, Korea*

[†]*These authors contributed equally to this work.*

**Corresponding authors (YHH – Fax, +82-42-865-3939; Email, hyh1127@kbsi.re.kr; HSK – Fax, +82-42-865-3939; Email, hskweon@kbsi.re.kr)*

Alzheimer's disease (AD) is a progressive neurodegenerative disorder. The deterioration of subcellular organelles, including the mitochondria, is another major ultrastructural characteristic of AD pathogenesis, in addition to amyloid plaque deposition. However, the three-dimensional (3-D) study of mitochondrial structural alteration in AD remains poorly understood. Therefore, ultrastructural analysis, 3-D electron tomography, and immunogold electron microscopy were performed in the present study to clarify the abnormal structural alterations in mitochondria caused by the progression of AD in APP/PSEN1 transgenic mice, expressing human amyloid precursor protein, as a model for AD. Amyloid β (Aβ) plaques accumulated and dystrophic neurites (DN) developed in the hippocampus of transgenic AD mouse brains. We also identified the loss of peroxiredoxin 3, an endogenous cytoprotective antioxidant enzyme and the accumulation of Aβ in the hippocampal mitochondria of transgenic mice, which differs from those in age-matched wild-type mice. The mitochondria in Aβ plaque-detected regions were severely disrupted, and the patterns of ultrastructural abnormalities were classified into three groups: disappearance of cristae, swelling of cristae, and bulging of the outer membrane. These results demonstrated that morpho-functional alterations of mitochondria and AD progression are closely associated and may be beneficial in investigating the function of mitochondria in AD pathogenesis.

[Choi KJ, Kim MJ, Je AR, Jun S, Lee C, Lee E, Jo M, Huh YH and Kweon H-S 2014 Three-dimensional analysis of abnormal ultrastructural alteration in mitochondria of hippocampus of APP/PSEN1 transgenic mouse. *J. Biosci.* **39** 97–105] **DOI** 10.1007/s12038-013-9406-8

1. Introduction

Alzheimer's disease (AD) is the most common age-related, progressive neurodegenerative disorder affecting millions of people worldwide; however, effective treatment for the aforementioned disease remains unavailable (Selkoe 2001; Mao and Reddy 2011). AD is characterized by severe loss of memory and cognitive functions (Manczak *et al*. 2010). The neuropathological hallmarks of AD include the accumulation of intracellular neurofibrillary tangles and the deposition of extracellular Aβ plaques (Nixon *et al.* 2005; Manczak *et al.* 2006). Neurofibrillary tangles and Aβ plaques have been found in the hippocampal region of the brain, which is responsible for learning and memory in AD patients and transgenic

Keywords. 3-D tomography; Alzheimer's disease; amyloid β; HVEM; mitochondria

Published online: 27 January 2014

AD mouse models (Reddy and Beal 2008; Reddy 2009; Kocherhans *et al.* 2010). AD is also characterized by dystrophic neurite (DN), synaptic damage and loss, and subcellular organelle dysfunction, including the mitochondria and the Golgi apparatus (Nixon *et al.* 2005; Manczak *et al.* 2006).

Mitochondria are regarded to play various roles in maintaining homeostasis in numerous organisms. In most cases, structural and functional mitochondrial disruptions directly affect disease progression (Hughes *et al.* 2003; Abdelwahid *et al.* 2007). Neuronal activity is sensitive to changes in mitochondrial function and extremely energy-dependent. The failure of homeostasis of mitochondrial energy metabolism induces reduction in ATP production and generation of reactive oxygen species (ROS) (Kann and Kovacs 2007; Piaceri *et al.* 2012). Moreover, mitochondrial bioenergetics and the bioenergetic homeostasis of brain metabolism affect Aβ processing (Brody *et al.* 2008; Kang *et al.* 2009). Using *in vivo* and *in vitro* approaches, recent studies have demonstrated that the interaction of Aβ peptide with the mitochondria and the subsequent accumulation of Aβ in the mitochondria are highly associated with mitochondrial dysfunction in damaged AD brains (Lin and Beal 2006; Manczak *et al.* 2006; Du *et al.* 2008). These accumulating evidences suggest that mitochondrial dysfunction and oxidative stress play an important role in the pathology of AD (Moreira *et al.* 2009).

Despite the important role of mitochondria in AD pathogenesis, the ultrastructural details of mitochondrial deterioration during AD progression remains poorly understood. In this study, we carefully analyzed mitochondrial protein expression and ultrastructure in the hippocampus of APP/PSEN1 double transgenic AD mice by immunogold labeling, high voltage electron microscopy (HVEM), and 3-D electron tomography. We found that the expression of peroxiredoxin 3 (Prx 3), an endogenous cytoprotective antioxidant enzyme, is reduced in Aβ-accumulated hippocampal mitochondria of transgenic mice, which is different from those in age-matched wild-type mice. We further showed that mitochondrial ultrastructure in Aβ plaque-detected regions were severely disrupted. We then classified the patterns of deteriorated mitochondrial structure into three groups: disappearance of cristae, swelling of cristae, and bulging of the outer membrane. These combined data suggest that the morpho-functional integrity of mitochondria is closely linked to AD progression.

2. Materials and methods

2.1 *Animals*

Seven-month-old homozygous APP/PSEN1 double transgenic mice and age-matched wild-type mice (B6C3F1/J background) were obtained from Jackson Laboratory (Bar Harbor, ME, USA). Animal studies were performed after obtaining approval from the Institutional Animal Care and Use Committee in the Korea Basic Science Institute (KBSI-ACE1013).

2.2 *Immunohistochemistry*

The animals were anesthetized with pentobarbital and transcardially perfused with phosphate buffered saline (PBS) and 4% paraformaldehyde at room temperature. The brains were then removed and postfixed in 4% paraformaldehyde/PBS and then placed in 30% sucrose in PBS overnight at 4°C. Serial coronal sections (10 μm) were obtained with a cryostat microtome (OTF5000, Bright, Cambridge, UK) and collected on glass slides, which were then stored at -20°C. Immunohistochemical investigations were performed according to the standard avidin-biotin-peroxidase method (Chi & Chandy, 2007). After the sections were blocked with 10% goat serum, they were incubated in the monoclonal anti-Aβ antibody (diluted 1:200; Abcam, Cambridge, MA, USA) overnight at 4°C and then washed in PBS containing 0.5% bovine serum albumin. The avidin-biotin-peroxidase method, with diaminobenzidine (DAB) as the chromogen was used to visualize the antibodies (brown reaction product).

2.3 *Conventional electron microscopy*

The brains were fixed in 2.5% glutaraldehyde in 0.1 M phosphate buffer (pH 7.4) for 2 hours at 4°C. After three washes in phosphate buffer, the tissues were postfixed with 1% osmium tetroxide on ice for 2 h and washed three times with phosphate buffer. The tissues were then embedded in Epon 812 after dehydration in an ethanol and propylene oxide series. Polymerization was conducted using pure resin at 70°C for two days. Ultrathin sections (70 nm) were obtained with an ultramicrotome (UltraCut-UCT, Leica, Austria), which were then collected on 100-mesh copper grids. After staining with 2% uranyl acetate (15 min) and lead citrate (5 min), the sections were examined by transmission electron microcopy (TEM) (Technai G^2 Spirit Twin, FEI, Hillsboro, OR, USA) at 120 kV.

2.4 *Pre-embedding immunogold electron microscopy*

For immunogold electron microscopy (EM), the brains were fixed with 4% paraformaldehyde and 0.05% glutaraldehyde in 0.1 M phosphate buffer (pH 7.4) overnight at 4°C. Coronal sections (100 μm) were cut with a vibratome (VT1000A, Leica, Vienna, Austria) and cryoprotected in 30% sucrose overnight at 4°C. The sections were incubated with monoclonal anti-Aβ antibody (1:200; Abcam, Cambridge, MA, USA) or polyclonal anti-Prx3 antibody (1:100; Ewha University, Seoul, Korea). The sections were then incubated with 1.4 nm gold particle-conjugated secondary antibodies. The specimens were reacted with a commercially available

GoldEnhanceTM-EM kit (Nanoprobes, New York, NY, USA) to enhance the signal from 1.4 nm gold particles. After signal enhancement, samples were postfixed in 1% osmium tetroxide for 1 h, dehydrated in ethanol, and flat-embedded in Epon 812. Polymerization was conducted using pure resin at 70°C for two days. Ultrathin sections (70 nm) were obtained with an ultramicrotome (UltraCut-UCT, Leica, Vienna, Austria) and subsequently collected on Formvar-coated single-hole copper grids. The sections were examined using TEM (Technai G^2 Spirit Twin, FEI, Hillsboro, OR, USA) at 120 kV after staining with 2% uranyl acetate (20 min) and lead citrate (10 min).

2.5 *Electron tomography and 3-D reconstruction*

The samples were sectioned (200 nm to 500 nm thick) for electron tomography of the hippocampal mitochondria from both wild-type and APP/PSEN1 transgenic mice. The sections were placed on the Formvar-coated copper grid, stained with 2% aqueous uranyl acetate and lead citrate, and the gold particles were placed on the surface of the sections to provide fiducial points for subsequent image alignment. After carbon coating to enhance the stability of the sample in the electron beam, the grid sections were placed on a tilting stage and viewed using a HVEM at 1250 kV (ARM-1300S, JEOL, Tokyo, Japan). The region of interest was selected and the sample was tilted from +60° to −60° with 2° increments. A total of 61 tilt images were recorded, and the digitized images were aligned using the gold particles in each tilt view as fiducial markers. Tomographic reconstruction from the tilt series was interpreted and modelled using the IMOD program package (Kremer *et al*., 1996). Virtual slices were extracted from the tomogram, and the boundaries of the region of interest that were visible in each tomographic slice were traced as contours overlaid on the image. The object surfaces were rendered using the AMIRA software (Visage Imaging, Carlsbad, CA, USA).

3. Results

3.1 *Ultrastructure of Aβ plaque and DN in the hippocampus of APP/PSEN1 transgenic mice*

We prepared brain sections from 7-month-old APP/PSEN1 transgenic mice and age-matched wild-type mice to study the deposition of Aβ plaque. Brain sections were immunolabeled

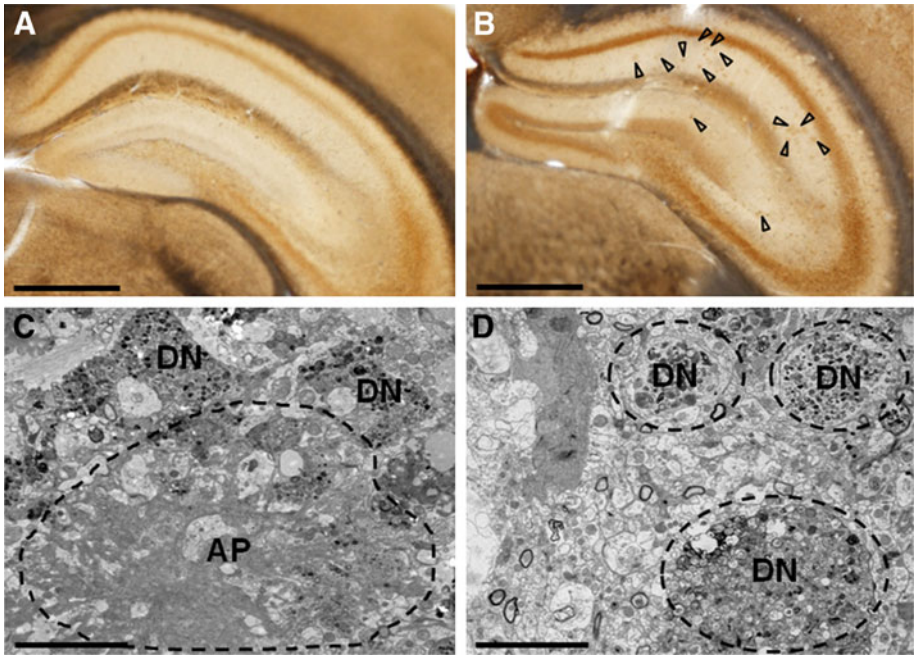

Figure 1. Light and electron microscopy images of Aβ plaque in the hippocampus of APP/PSEN1 transgenic mouse brain. (**A**–**B**) Representative light microscopic images of sagittal half-brain sections of wild-type (**A**) and APP/PSEN1 transgenic mice (**B**). Aβ plaques in the hippocampus of the APP/PSEN1 transgenic mice (arrows in **B**) were immunolabeled with the anti-Aβ antibody and visualized with DAB, as described in Materials and methods. Note that the immunolabeled Aβ deposits (arrows) were detected in the brain of the APP/PSEN1 transgenic mice. (**C**–**D**) Electron micrographs of the Aβ plaque core in the hippocampus of the APP/PSEN1 transgenic mouse brain. Representative micrographs were acquired from the anti-Aβ antibody-positive Aβ plaque region in (**B**). AP, Aβ plaque (dotted circle in **C**); DN, dystrophic neurite (dotted circles in **D**). Scale bars = 150 μm (**A** and **B**) and 5 μm (**C** and **D**).

with Aβ selective anti-Aβ antibody and detected by DAB immunoperoxidase reactions. We found that circular-shaped Aβ plaques accumulated in the hippocampus (figure 1B) of the APP/PSEN1 transgenic mice brain, which was different from that of the age-matched wild-type mice brain (figure 1A). The Aβ-positive hippocampal regions of the APP/PSEN1 transgenic mice brain in figure 1B were then analyzed using TEM to characterize the ultrastructural features of the Aβ plaque deposits (figure 1C) and dystrophic neurites (figure 1D). The ultrastructural feature of the Aβ plaque core exhibits a star-shaped appearance with spokes of amyloid extending outward and a core surrounded by several dystrophic neurites (figure 1C). Abnormally enlarged dystrophic neurites were filled mainly with various vesicular and membranous structures, showing different electron densities (figure 1D).

3.2 *Alteration of protein expression in APP/PSEN1 transgenic mice*

We subsequently examined the expression of Prx 3 and Aβ on the mitochondria in the hippocampus of transgenic mice by immunogold EM analysis to check whether the expression of endogenous antioxidant enzyme in mitochondria is affected by the deposition of Aβ and whether functional damage induces structural alteration in mitochondria (figure 2). The gold particles targeting Prx 3 were mostly localized in the mitochondrial cristae and inner/outer membranes in the wild-type mice (figure 2A, top left). However, significantly less specific reactivity to Prx 3 was observed in the mitochondrial cristae and the inner/outer membranes of the APP/PSEN1 transgenic mice (figure 2A, top right). In detail, the number of Prx 3-targeting gold particles per mitochondrial area (mm^2) of wild-type mice and APP/PSEN1 transgenic mice is 9.50±0.97 and 1.7±0.50, respectively (figure 2B). Interestingly, the accumulation of Aβ in the cristae of disrupted mitochondria in transgenic mice was detected (figure 2A, bottom right), which was different from that of the wild-type mice (figure 2A, bottom left).

3.3 *Alteration patterns of mitochondrial structure in APP/PSEN1 transgenic mice*

The relevance of mitochondrial dysfunction in the progression of neurodegenerative diseases including AD has been proposed in various animal models (Baloyannis, 2006; Umeda *et al.* 2011). However, the various patterns of ultrastructural alteration in mitochondria at the TEM level were not reported in detail. Therefore, we focused on the classification of

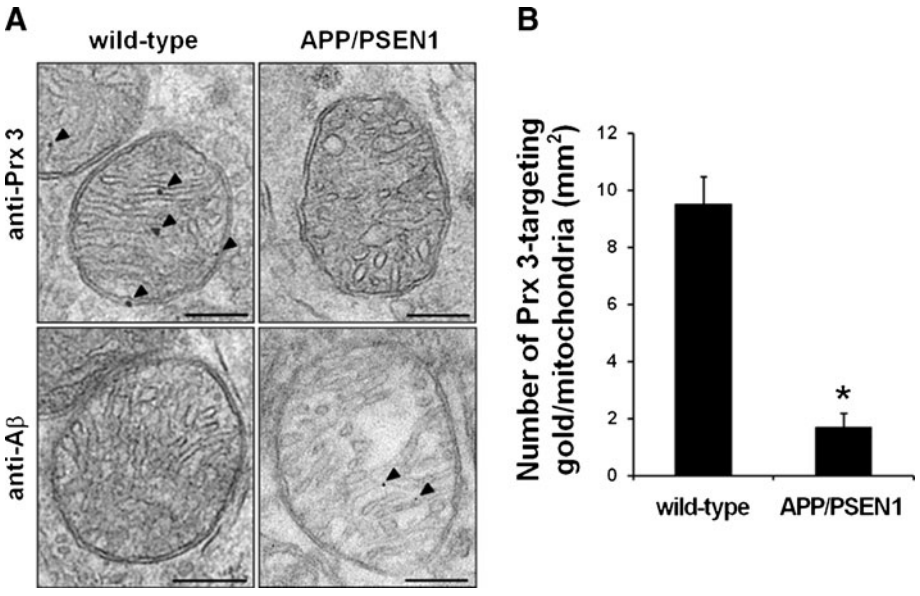

Figure 2. Immunogold labeling of Prx 3 and Aβ in hippocampal mitochondria of APP/PSEN1 transgenic mice. (**A**) Representative images of Prx 3 (top panel) and Aβ (bottom panel) detected in the hippocampal mitochondria of wild-type and APP/PSEN1 transgenic mice are shown. Scale bars = 200 nm. (**B**) Quantitative summary for the expression of Prx 3 per mm^2 of hippocampal mitochondria area between the wild-type mice and the APP/PSEN1 transgenic mice. Immuno-nanogold/gold enhancement labeling were performed using anti-Prx 3 and anti-Aβ antibodies. The results are expressed as mean±SEM. Number of mitochondria examined are 80 in each column. * denotes significant (P<0.001) difference from that of the wild-type mice (Student's t-test).

ultrastructural alteration patterns of mitochondria in APP/PSEN1 transgenic mice. Normal mitochondria maintain a dense matrix compacted with thin and uniform cristae and surrounded by clear inner and outer membranes (figure 3A). However, most mitochondria from the transgenic mice showed various patterns of structural abnormalities, and these structural variations were classified into three groups: disappearance of cristae (figure 3B), swelling of cristae (figure 3C), and bulging of the outer membrane (figure 3D).

We then investigated the ultrastructural alteration pattern of mitochondria in three-dimensions by HVEM and electron tomography (figure 4). Through the reconstructed 3-D models, we further confirmed the structural abnormalities of mitochondria in APP/PSEN1 transgenic mice compared with the wild-type mice (figure 4A). In structurally deteriorated mitochondria, the cristae severely disappeared through the entire mitochondria (figure 4B). The remaining fragmented cristae in the disrupted mitochondria were also swollen (figure 4C). In few cases, the outer membrane of the mitochondria bulged out (figure 4D).

Then, we counted the number of mitochondria in each group, based on the images that taken from both the APP/PSEN1 transgenic mice and the age-matched wild-type mice. In the wild-type mice, 83.22% (548/657) of the mitochondria maintained their normal structure and 17.32% of the mitochondria exhibited structural abnormalities such as the disappearance of cristae (10.57%, 68/657), swelling of cristae (5.46%, 36/657), and bulging of the outer membrane (0.75%, 5/657) (WT of figure 5A). Interestingly, the number of normal mitochondria in the APP/PSEN1 transgenic mice sharply decreased to 55.07% (271/491). On the other hand, the population of abnormal mitochondria exhibiting disappearance of cristae (30.15%, 148/491), swelling of cristae (13.13%, 64/491), and bulging of the outer membrane (1.65%, 8/491) significantly increased compared with the wild-type mice (TG of figure 5A). Next, we relatively compared each ultrastructural pattern found in mitochondria of the wild-type and the APP/PSEN1 transgenic mice. For comparison, the number of mitochondria for each ultrastructural pattern in the wild-type mice was normalized to 100%. The number of normal mitochondria in the APP/PSEN1 transgenic mice (66.2±6.4%) was significantly lower than that of the wild-type mice. Whereas, the abnormal mitochondria showing the disappearance of cristae, swelling of cristae, and bulging of the outer membrane in the APP/PSEN1 transgenic mice significantly increased to 285.24±26.48%,

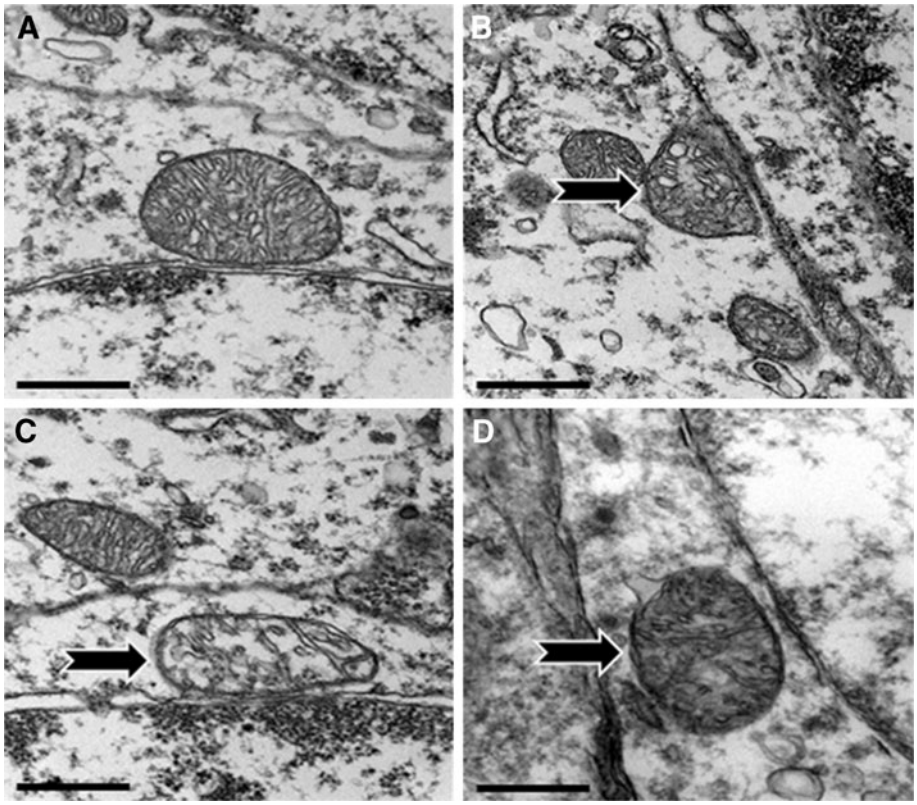

Figure 3. Various ultrastructural patterns of mitochondrial abnormalities in the hippocampus of APP/PSEN1 transgenic mice. Representative images taken from the Aβ plaque-detected region of the hippocampus. (**A**) normal structure of mitochondria. (**B**–**D**) Various mitochondrial abnormalities are shown (arrows), such as disappearance of cristae (**B**), swelling of cristae (**C**), and bulging of the outer membrane (**D**).

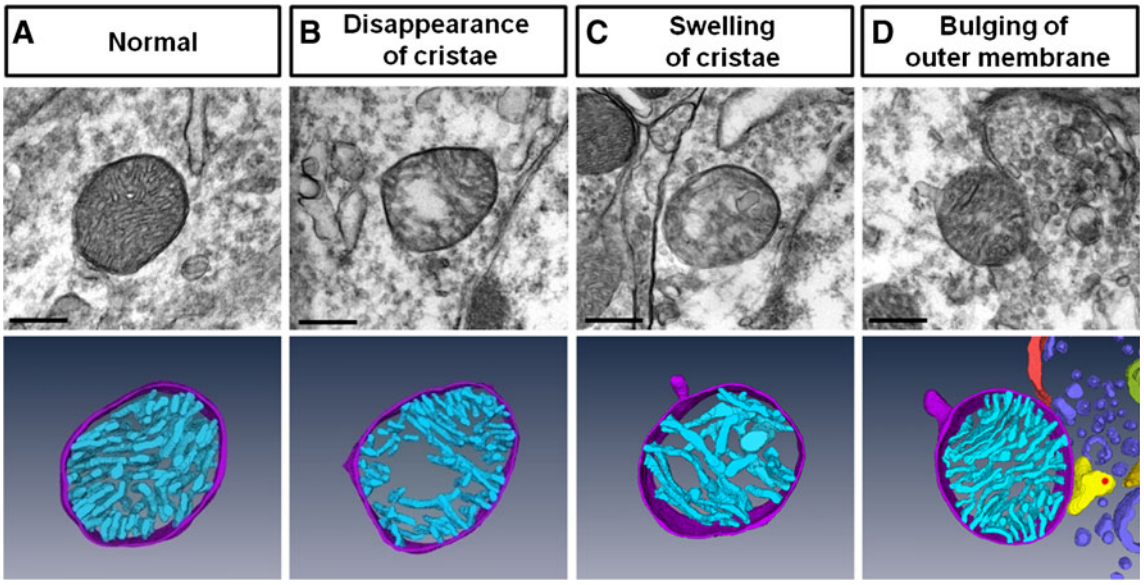

Figure 4. Three-dimensional reconstruction of sections with thicknesses ranging from 0.2 to 0.5 μm of the hippocampal mitochondria from APP/PSEN1 transgenic mice. The tilt series containing 61 images were recorded over a tilt range of −60° to 60°, with an interval of 2° by HVEM. (**A**) Representative image of normal mitochondria. (**B**–**D**) Examples of abnormal mitochondria, showing the disappearance of cristae (**B**), swelling of cristae (**C**), and bulging of the outer membrane (**D**). Top row: The 0° images of mitochondria were acquired by HVEM. Bottom row: Object surfaces of tomogram were rendered using the AMIRA software (Visage Imaging). The outer and inner membranes of the mitochondria were represented in violet, and the cristae were represented with cyan colors. Scale bar = 500 nm.

243.16±15.52%, and 219.99±73.33%, respectively, compared with those of the wild-type mice (figure 5B). However, the number of mitochondria in wild-type mice and APP/PSEN1 transgenic mice is quite similar, that is, the mitochondria number per 100 μm^2 of wild-type mice and APP/PSEN1 transgenic mice is 5.76±0.34 and 5.3±0.37, respectively.

4. Discussion

In this study, we investigated the functional and structural alteration in mitochondria of the hippocampus of APP/PSEN1 double transgenic mice, which is a well-established transgenic mouse model of AD. We performed conventional TEM, 3-D electron tomography, and immunogold EM analysis to clarify the effects of Aβ accumulation on the functional and ultrastructural alterations of mitochondria in APP/PSEN1 double transgenic mice. We confirmed the presence of Aβ plaque in the hippocampus of AD mice (figure 1), and the endogenous protein expression and ultrastructure of the mitochondria in Aβ plague-accumulated hippocampal regions have evidently deteriorated (figures 2 to 5). The results of our study demonstrated that mitochondrial protein expression and related ultrastructure in the Aβ-accumulated region is remarkably changed in the hippocampus of AD mice.

Despite various studies, the effect of mitochondrial Aβ on the maintenance of mitochondrial homeostasis could not be confirmed because of lack of direct evidence, although Aβ has been demonstrated in mitochondrial damage, both functionally and structurally (Trimmer *et al.* 2000; Keil *et al.* 2004; Reddy and Beal 2008; Kim *et al.* 2012). In AD, mitochondrial abnormalities are partly attributed to the spectrum of chronic oxidative stress in AD (Hirai *et al.* 2001). During AD progression, toxic Aβ peptides are targeted and localized to the mitochondrial matrix and cristae (Anandatheerthavarada *et al.* 2003; Petersen *et al.* 2008). These peptides then inhibit the function of alcohol dehydrogenase by binding with this enzyme at the mitochondrial matrix and facilitate the generation of mitochondrial ROS (Baloyannis 2006; Umeda *et al.* 2011). ROS-induced mitochondrial dysfunctions such as changes in mitochondrial membrane potential, release of cytochrome C in the cytoplasm, and alteration in mitochondrial structure and protein expression then occur (Manczak *et al.* 2006; Kim *et al.* 2012).

Mammalian cells are equipped with detoxifying enzymes, including catalase, glutathione peroxidases (GPxs), and peroxiredoxins to protect the cells from ROS-induced toxicity (Woo *et al.* 2010). In the mitochondria, proper expression and function of peroxiredoxin 3 is extremely important for maintaining not only the mitochondrial function itself but the related cell and tissue functions as well (Hattori *et al.* 2003; Kil *et al.* 2012; Lijnen *et al.* 2012). In the present study, Prx 3 expression in the mitochondria of APP/PSEN transgenic mice was shown to be quite different from that of the wild-type mice. Also the expression patterns of Aβ and Prx 3 were opposite. Aβ was

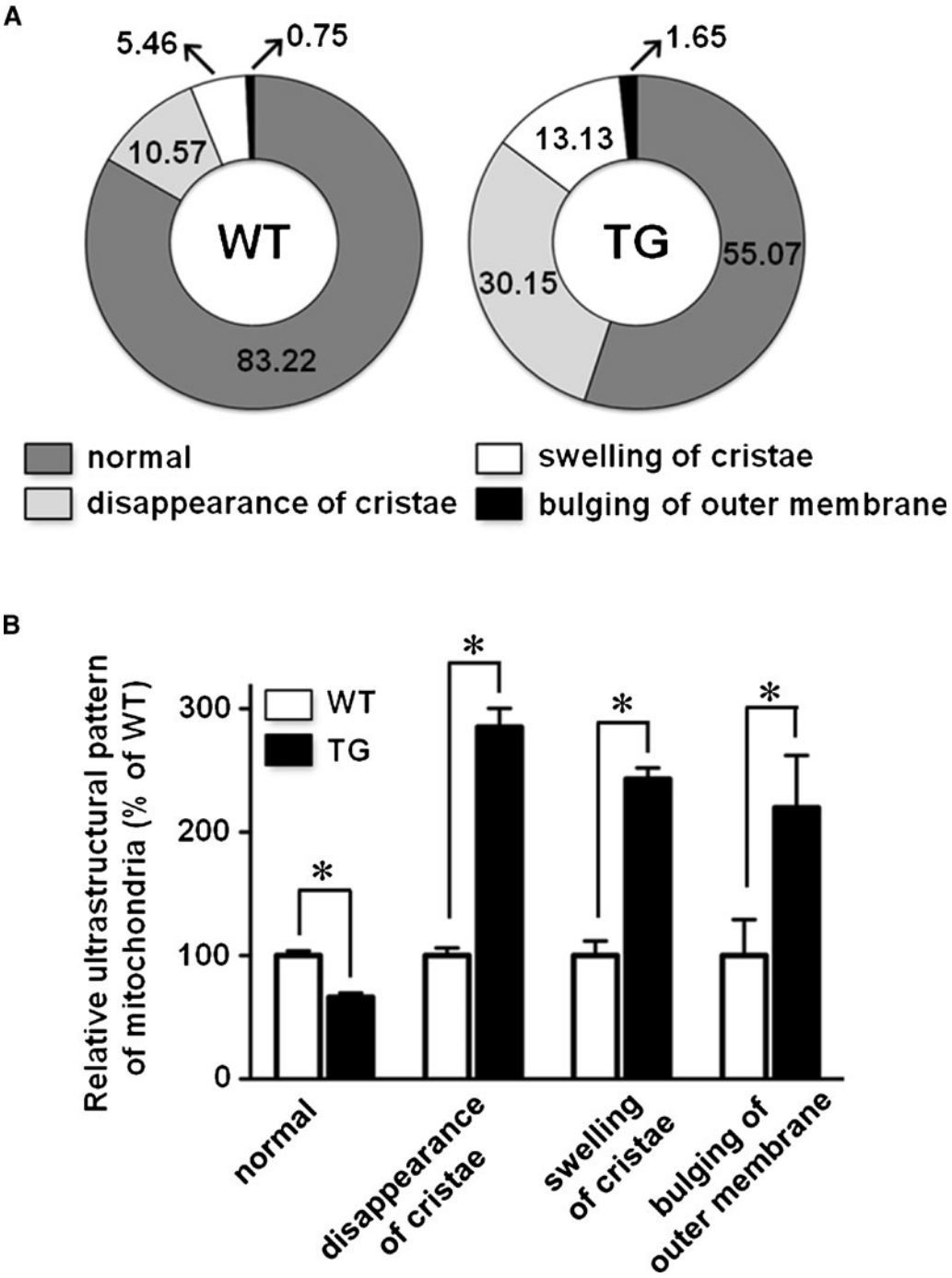

Figure 5. Quantitative summary for the alteration patterns in mitochondrial structures of wild-type and APP/PSEN1 transgenic mice. (**A**) Comparison of the component ratio of normal and abnormal mitochondrial ultrastructure of wild-type and APP/PSEN transgenic mice. (**B**) Quantitative summary for the relative comparison of the ultrastructural mitochondrial pattern between the wild-type and the APP/PSEN1 transgenic mice. For the comparison, the number of mitochondria for each of the ultrastructural pattern in the wild-type mice was normalized to 100%. The results are expressed as mean±SEM (n=15). * denotes significant (P<0.001) difference from that of the wild-type mice. WT, wild-type mice; TG, APP/PSEN1 transgenic mice.

localized in the mitochondrial cristae in APP/PSEN1 transgenic mice. Interestingly, Prx 3 was endogenously expressed in the mitochondrial cristae and inner/outer membranes in the wild-type mice but was diminished in the mitochondria of transgenic mice (figure 2). Therefore, the morpho-functional deterioration of mitochondria of APP/PSEN1 transgenic mice may be partly attributed to Aβ toxicity and Prx 3 loss-induced oxidation. Furthermore, the ultrastructure of mitochondrial membranes and cristae in the hippocampus of APP/PSEN1 transgenic mice were severely disrupted (figures 3 and 4). This alteration in structural and functional integrity is closely associated with the maintenance of mitochondrial volume homeostasis (Kaasik *et al*. 2007). Kaasik and colleagues (2007) suggested the hypothetical phases of mitochondrial swelling, including the expansion of mitochondrial matrix with or without mitochondrial shape remodeling and rupture of the outer membrane or mitochondrial fusion. In our study, the expansion of mitochondrial matrix was observed by the disappearance of cristae and the rupture and/or bulge of the mitochondrial membrane (figures 3 and 4); however, remarkable change in mitochondrial size or remodeling of mitochondrial shape was not observed.

In addition, we compared the number of mitochondria between wild-type mice and APP/PSEN1 transgenic mice. In difference with the another Alzheimer's disease model, Tg2576 mice (Balietti *et al.* 2013) that the number of mitochondria is increased compared to wild type, in our study, the number of mitochondria per 100 μm^2 is quite similar in wild-type mice and APP/PSEN1 transgenic mice. This difference maybe caused in part by age difference and strain difference between two studies. However, further study on the changes of mitochondria number between wild-type mice and APP/PSEN1 transgenic mice seems to be needed.

According to several reports on AD that used TEM, toxic Aβ-mediated functional and structural abnormalities of the mitochondria include changes in mitochondrial volume, structure, and protein expression (Trimmer *et al.* 2000; Hirai *et al.* 2001; Anandatheerthavarada *et al.* 2003; Petersen *et al*. 2008). During apoptosis or postnatal stenosis, similar patterns of abnormalities in the mitochondrial ultrastructure were also reported, and these ultrastructural damages were closely related with cell death and disease progression (Hughes *et al.* 2003; Abdelwahid *et al.* 2007). Based on the mitochondrial structure reported in the cited articles, the ultrastructural abnormalities of the mitochondria can be classified into typical patterns, such as swelling with a round shape, less dense matrix, disorganized or broken cristae, and membrane disruption and bulging. In the present study, mitochondrial abnormalities in the hippocampus of APP/PSEN1 double transgenic AD model mouse exhibit patterns quite similar to those listed above, and the patterns of ultrastructural abnormalities are classified into three groups, including the disappearance of cristae, swelling of cristae, and bulging of the outer membrane (figures 3 and 4). However, whether these patterns of abnormalities are caused by independent processes or a sequence of breaking step remains unknown. Nonetheless, according to our recent immune EM analysis, detached membraneous components near the mitochondria, which show patterns of structural abnormality, are positively stained with anti-Prx 3 antibodies. Simultaneously, Prx 3-positive signals were also detected in the membraneous components that accumulated in the autophagosome-compacted dystrophic neuritis (data not shown). Therefore, the fragmented membraneous compartments of mitochondria appear to move into dystrophic neuritis through the cytoplasm and are subsequently digested by autophagosomes. However, further studies must be conducted to understand how the fragmented mitochondrial membranes are moved to dystrophic neuritis and how these fragments were digested by autophagosomes in dystrophic neuritis.

In this study, we reported various ultrastructural alterations in mitochondria near the Aβ-deposited AD region located in the hippocampus of APP/PSEN1 double transgenic mice. The present results confirm the understanding that the abnormal ultrastructural alterations in mitochondria are closely associated with the development of AD. However, further studies are required to investigate the precise molecular mechanisms related to Aβ-induced functional and morphological changes of the mitochondria, as well as the digestion of fragmented mitochondrial membrane compartments in dystrophic neuritis during AD pathogenesis.

Acknowledgements

This research was supported by Korea Basic Science Institute grant (T32404) and the National Research Foundation of Korea (NRF), and was funded by the Ministry of Education, Science and Technology (MEST) of Korea (2009, University-Institute cooperation program). We thank HA Woo for providing Prx-3 antibody.

References

Abdelwahid E, Yokokura T, Krieser RJ, Balasundaram S, Fowle WH and White K 2007 Mitochondrial disruption in *Drosophila* apoptosis. *Dev. Cell* **12** 793–806

Anandatheerthavarada HK, Biswas G, Robin MA and Avadhani NG 2003 Mitochondrial targeting and a novel transmembrane arrest of Alzheimer's amyloid precursor protein impairs mitochondrial function in neuronal cells. *J. Cell Biol.* **161** 41–54

Balietti M, Giorgetti B, Casoli T, Solazzi M, Tamagnini F, Burattini C, Aicardi G and Fattoretti P 2013 Early selective vulnerability of synapses and synaptic mitochondria in the hippocampal CA1 region of the Tg2576 mouse model of Alzheimer's disease. *J. Alzheimers Dis.* **34** 887–896

Baloyannis SJ 2006 Mitochondrial alterations in Alzheimer's disease. *J. Alzheimers Dis.* **9** 119–126

Brody DL, Magnoni S, Schwetye KE, Spinner ML, Esparza TJ, Stocchetti N, Zipfel GJ and Holtzman DM 2008 Amyloid-beta dynamics correlate with neurological status in the injured human brain. *Science* **321** 1221–1224

Chi V and Chandy KG 2007 Immunohistochemistry: paraffin sections using the Vectastain ABC kit from vector labs. *J. Vis. Exp.* **8** 308

Du H, Guo L, Fang F, Chen D, Sosunov AA, Mckhann GM, Yan Y, Wang C, *et al.* 2008 Cyclophilin D deficiency attenuates mitochondrial and neural perturbation and ameliorates learning and memory in Alzheimer's disease. *Nat. Med.* **14** 1097–1105

Hattori F, Murayama N, Noshita T and Oikawa S. 2003 Mitochondrial peroxiredoxin-3 protects hippocampal neurons from excitotoxic injury *in vivo*. *J. Neurochem*. **86** 860–868

Hirai K, Aliev G, Nunomura A, Fujioka H, Russel RL, Atwood CS, Johnson AB and Kress Y *et al.* 2001 Mitochondrial abnormalities in Alzheimer's disease. *J. Neurosci.* **21** 3017–3023

Hughes DE, Stolz DB, Yu S, Tan Y, Reddy JK, Watkins SC, Diehl AM and Costa RH 2003 Elevated hepatocyte levels of the forkhead box A2 (HNF-3β) transcription factor cause postnatal steanosis and mitochondrial damage. *Hepatology* **37** 1414–1424

Kaasik A, Safiulina D, Zharkovsky A and Veksler V 2007 Regulation of mitochondrial matrix volume. *Am. J. Physiol. Cell Physiol.* **292** 157–163

Kann O and Kovacs R 2007 Mitochondria and neuronal activity. *Am. J. Physiol. Cell Physiol.* **292** 641–657

Kang JE, Lim MM, Bateman RJ, Lee JJ, Symth LP, Cirrito JR, Fujiki N, Nishino S, *et al.* 2009 Amyloid-beta dynamics are regulated by orexin and the sleep-wake cycle. *Science* **326** 1005–1007

Keil U, Bonert A, Marques CA, Scherping I, Weyermann J, Strosznajder JB, Müller-Spahn F, Haass C, *et al.* 2004 Amyloid beta-induced changes in nitric oxide production and mitochondrial activity lead to apoptosis. *J. Biol. Chem*. **279** 50310–50320

Kil IS, Lee SK, Ryu KW, Woo HA, Hu MC, Bae SH and Rhee SG 2012 Feedback control of adrenal steroidogenesis via H_2O_2-dependent, reversible inactivation of peroxiredoxin III in mitochondria. *Mol. Cell* **46** 584–594

Kim MJ, Huh YH, Choi KJ, Jun S, Je AR, Chae H, Lee C and Kweon HS 2012 Ultrastructural abnormalities in APP/PSEN1 transgenic mouse brain as the Alzheimer's disease model. *Appl. Microsc.* **42** 179–185

Kocherhans S, Madhusudan A, Doehner J, Breu KS, Nitsch RM, Fritschy JM and Knuesel I 2010 Reduced Reelin expression accelerates amyloid-beta plaque formation and tau pathology in transgenic Alzheimer's disease mice. *J. Neurosci*. **30** 9228–9240

Kremer JR, Mastronarde DN and Mclntosh J 1996 Computer visualization of three-dimensional image data using IMOD. *J. Struct. Biol.* **116** 71–76

Lijnen PJ, Piccart Y, Coenen T and Prihadi JS 2012 Angiotensin II-induced mitochondrial reactive oxygen species and peroxiredoxin-3 expression in cardiac fibroblasts. *J. Hypertens*. **30** 1986–1991

Lin MT and Beal MF 2006 Alzheimer's APP mangles mitochondria. *Nat. Med.* **12** 1241–1243

Manczak M, Mao P, Calkins MJ, Cornea A, Reddy AP, Murphy MP, Szeto HH and Park B *et al.* 2010 Mitochondria-targeted antioxidants protect against Abeta toxicity in Alzheimer's disease neurons. *J. Alzheimers Dis.* **20** 609–631

Manczak M, Anekonda TS, Henson E, Park BS, Quinn J and Reddy PH 2006 Mitochondria are a direct site of A beta accumulation in Alzheimer's disease neurons: implications for free radical generation and oxidative damage in disease progression. *Hum. Mol. Genet.* **15** 1437–1449

Mao P and Reddy PH 2011 Aging and amyloid beta-induced oxidative DNA damage and mitochodrial dysfunction in Alzheimer's disease: implications for early intervention and therapeutics. *Biochim. Biophys. Acta* **1812** 1359–1370

Moreira PI, Duarte AI, Santos MS, Rego AC and Oliveira CR 2009 An integrative view of the role of oxidative stress, mitochondria and insulin in Alzheimer's disease. *J. Alzheimers Dis.* **16** 741–761

Nixon RA, Wegiel J, Kumar A, Yu WH, Peterhoff C, Cataldo A and Cuervo AM 2005 Extensive involvement of autophagy in Alzheimer disease: an immuno-electron microscopy study. *J. Neuropathol. Exp. Neurol.* **64** 113–122

Petersen CAH, Alikhani N, Behbahani H, Wiehager B, Pavlov PF, Alafuzoff I, Leinonen V and Ito A *et al.* 2008 The amyloid β-peptide is imported into mitochondria via the TOM import machinery and localized to mitochondrial critae. *Proc. Natl. Acad. Sci. USA* **105** 13145–13150

Piaceri I, Rinnochi V, Bagnoli S, Failli Y and Sorbi S 2012 Mitochondria and Alzheimer's disease. *J. Neurol. Sci*. **322** 31–34

Reddy PH 2009 Amyloid beta, mitochondrial structural and functional dynamics in Alzheimer's disease. *Exp. Neurol.* **218** 286–292

Reddy PH and Beal MF 2008 Amyloid beta, mitochondrial dysfunction and synaptic damage: implications for cognitive decline in aging and Alzheimer's disease. *Trends Mol. Med.* **14** 45–53

Selkoe DJ 2001 Alzheimer's disease: genes, proteins, and therapy. *Physiol. Rev*. **81** 741–766

Trimmer PA, Swerdlow RH, Parks JK, Keeney P, Bennett JP Jr, Miller SW, Davis RE and Parker WD Jr 2000 Abnormal mitochondrial morphology in sporadic Parkinson's and Alzheimer's disease cybrid cell lines. *Exp. Neurol.* **162** 37–50

Umeda T, Tomiyama T, Sakama N, Tanaka S, Lambert MP, Klein WL and Mori H 2011 Intraneuronal amyloid β oligomers cause cell death via endoplasmic reticulum stress, endosomal/lysosomal leakage, and mitochondrial dysfunction *in vivo*. *J. Neurosci. Res.* **89** 1031–1042

Woo HA, Yim Sh, Shin DH, Kang D, Yu DY and Rhee SG 2010 Inactivation of peroxiredoxin I by phosphorylation allows localized H_2O_2 accumulation for cell signalling. *Cell* **140** 517–528

MS received 22 April 2013; accepted 14 November 2013

Corresponding editor: VIDITA A VAIDYA